Article ID: 1000-7032(2025)07-1249-13

White Light Emission Enhancement in Sm^{3+}-doped Lithium Aluminum Silicate Glasses by Ag Nanoparticles

CHANG Yuanxing[1], ZHANG Dandan[1], YIN Guanchao[1], WANG Yesen[1], WANG Mingzhong[1,2], QIU Jianbei[3], XU Yinsheng[1*]

(1. *State Key Laboratory of Silicate Materials for Architectures, Wuhan University of Technology, Wuhan* 430070, *China*;
2. *Yichang CSG photoelectric Glass Co., Ltd., Yichang* 443000, *China*;
3. *College of Materials Science and Engineering, Kunming University of Science and Technology, Kunming* 650000, *China*)
* *Corresponding Author, E-mail: xuyinsheng@whut. edu. cn*

Abstract: Sm^{3+}-doped materials exhibit red and orange emissions in the visible light region, showing broad application prospects in both laser and display material fields. However, the inherent small emission and absorption cross-sections of Sm^{3+} result in low luminous efficiency, posing challenges for achieving high-quality solid-state lighting. Here, the excellent white emission of Sm^{3+} doped lithium aluminum silicate (LAS) glass was realized by introducing the Ag aggregates through Ag ion exchange. Under 395 nm excitation, the Ag-doped samples exhibit significant fluorescence enhancement with color coordinates close to the equal energy white point E (0. 33, 0. 33) and a color rendering index (CRI) of 81. 8. The study reveals that the surface plasmon resonance (SPR) effect of Ag nanoparticles enhances the luminescence of Sm^{3+}, while the energy transfer mechanism between Ag^{+} and Sm^{3+} also promotes fluorescence enhancement. By adjusting the concentration of $AgNO_3$ and the exchange time, a series of high-quality full-spectrum white light emissions were obtained, indicating that the Ag ion-exchanged Sm^{3+}-doped LAS glass has good application potential in the development of solid-state lighting devices. Moreover, variations in the excitation wavelength can effectively tune the emission color, further demonstrating the tunability and practicality of this material in optoelectronic applications.

Key words: Ag NPs; luminescent properties; rare earth ions; lithium aluminum silicate glass
CLC number: O433. 54 **Document code**: A
DOI: 10. 37188/CJL. 20250047 **CSTR**: 32170. 14. CJL. 20250047

银纳米颗粒增强钐掺杂锂铝硅玻璃的白光发射

常元星[1], 张丹丹[1], 殷官超[1], 王业森[1], 王明忠[1,2], 邱建备[3], 许银生[1*]

(1. 武汉理工大学 硅酸盐科学与先进建材全国重点实验室, 湖北 武汉 430070;
2. 宜昌南玻光电玻璃有限公司, 湖北 宜昌 443000;
3. 昆明理工大学 材料科学与工程学院, 云南 昆明 650000)

摘要: 掺杂Sm^{3+}的材料在可见光区域会发出红色和橙色光,在激光和显示材料领域具有广阔的应用前景。然而,Sm^{3+}固有的小发射和吸收截面导致其发光效率较低,为实现高质量的固态照明带来了挑战。本文通过银离子交换引入银聚集体,实现了掺杂Sm^{3+}的硅酸铝锂(LAS)玻璃的优异白光发射。在 395 nm 激发下,银离子交换样品的荧光显著增强,色坐标接近等能量白点 E(0.33, 0.33),显色指数(CRI)为 81.8。研究发现,Ag 纳米颗粒的表面等离子体共振(SPR)效应增强了Sm^{3+}的发光,而Ag^{+}与Sm^{3+}之间的能量传递机制也促进了荧光增

收稿日期: 2025-02-27; **修订日期**: 2025-03-23
基金项目: 国家自然科学基金(U2241236)
Supported by National Natural Science Foundation of China (U2241236)

强。通过调节 $AgNO_3$ 的浓度和交换时间，获得了一系列高质量的全光谱白光发射，表明 Ag 离子交换 Sm^{3+} 掺杂的 LAS 玻璃在固态照明器件的开发中具有良好的应用潜力。此外，激发波长的变化可以有效调节发射颜色，进一步证明了这种材料在光电应用中的可调性和实用性。

关 键 词：银纳米颗粒；发光特性；稀土离子；锂铝硅酸盐玻璃

1 Introduction

The absorption of light by rare earth ions (REIs) occurs through transitions between different energy levels of the inner 4f electrons[1-2], resulting in numerous absorption and emission spectral lines that can emit light ranging from UV, visible to infrared wavelengths[3-4]. The fluorescence lifetime spans 6 orders of magnitude, from nanoseconds to milliseconds. It is these exceptional properties that make rare earth compounds indispensable in various fields such as lasers, scintillation materials, display materials, and lighting[5-7]. Among the numerous REIs, Sm^{3+} exhibits red and orange emissions in the visible light region, and Sm^{3+}-doped glass has been utilized as a high-power light source in microbeam radiotherapy for preclinical radiation therapy for cancer[8]. Additionally, it finds applications in underwater communication, high-density optical storage, color displays, and solid-state laser in the visible light region[9-11]. However, the inherently small emission and absorption cross-sections of Sm^{3+} ions lead to low luminescent efficiency, thereby limiting their practical applications.

It has been proved that the luminescence of REIs in glass can be effectively enhanced by Ag nanoparticles (Ag NPs)[12-13]. Kindrat *et al*. found that the luminescence of Eu^{3+} can be significantly enhanced by incorporating Ag NPs into fluoborate glass[14]. Currently, the mechanisms by which Ag NPs enhance the luminescence of REIs are primarily classified into two categories. One is attributed to the local field enhancement (LFE) induced by the surface plasmon resonance (SPR) of Ag NPs, which enhances the electromagnetic field surrounding Sm^{3+}, leading to fluorescence enhancement[15-16]. The other is attributed to energy transfer (ET) from small molecular aggregates of Ag_m^{n+} or free Ag^+ to REIs[17]. Besides enhancing the luminescence of REIs, Ag NPs also provide pathways for non-radiative loss of excitation energy, resulting in photoluminescence (PL) quenching effects[18]. Overall, the interaction between Ag species and REIs is quite complex, and the actual mechanism remains controversial, necessitating further investigation.

Compared to phosphors and crystalline materials, glass is an important optoelectronic material due to its high transparency and ease of processing[19-23]. There are two methods for doping Ag NPs into glass: doping during melting and ion-exchange. The doping concentration of the former is generally low, suitable for the preparation of photosensitive glass and polarizing glass. The latter achieves a higher doping concentration, and the ion-exchange process can effectively control the state of Ag in the glass through factors such as molten salt content, exchange temperature, and exchange time, making it an effective method to obtain the desired Ag state[24].

During the ion-exchange process, Ag^+ replace Na^+ and Li^+ in the glass and gradually penetrate into the interior of the glass, forming complex luminescent centers such as Ag^+, Ag^+-Ag^+, and Ag nanoclusters (Ag NCs). These Ag aggregates exhibit a broad emission band spanning the blue to red region (350 nm to 610 nm)[25]. When combined with Sm^{3+} emitting red light, Ag species can provide blue-green spectral components, thereby achieving white light emission. Meanwhile, the emission band of Ag NCs can provide broadband white light with high-quality parameters such as a high CRI. Therefore, introducing Ag species into Sm^{3+}-doped LAS glass through the ion-exchange process is a feasible method to achieve high-quality white light emission.

In this study, Sm^{3+}-doped LAS glass was prepared using the melt-quenching method. Among

alkali metal ions, Li^+ ions exhibit the smallest size. Based on the "filling effect" of ion-exchange, Li-containing glasses demonstrate robust ion-exchange capabilities. LAS possesses excellent optical transparency, good chemical stability, low coefficient of thermal expansion, high strength, and high hardness, enabling ion-exchange without compromising transparency. Consequently, Ag was introduced into the prepared rare-earth ion (REI)-doped glasses through ion-exchange between Ag^+ and Li^+ and Na^+ ions, forming complex optical centers involving Sm^{3+} and various Ag^+ ion species. By adjusting the ion-exchange time and the ratio of $c(NaNO_3)/c(AgNO_3)$ in the molten salt, a series of high-quality white light emissions across the entire visible spectrum were achieved, with a CRI reaching 81.8. Furthermore, the emission spectra were effectively tuned by varying the excitation wavelength, suggesting that the selection of excitation wavelength is a feasible approach to optimize the luminescent color of Sm^{3+}. The tunability of the glass fluorescence color indicates that Sm^{3+}-doped LAS glasses subjected to Ag^+-Na^+ ion-exchange hold great potential for developing WLED lighting devices[26-27].

2　Experiment

2.1　Glass Preparation

30 g LAS glass was prepared using raw materials with a purity of 99.99% purchased from Shanghai Aladdin Biochemical Technology Co., Ltd. and China National Pharmaceutical Group Chemical Reagents Co., Ltd. The main glass molar composition is 64 SiO_2-12 Al_2O_3-2 ZrO_2-10 Li_2CO_3-10 Na_2CO_3-1 H_3BO_3-1 MgO-1 K_2CO_3. 0.4% Sm_2O_3 (mole fraction) was doped in the glass as the luminous center, the sample without Sm_2O_3 doping is labeled as S0, while the sample doped with 0.4% Sm_2O_3 is labeled as S4. The raw materials were combined in an agate mortar and ground for 30 min to ensure a homogeneous mixture. The resulting mixture was then transferred into an alumina crucible and melted in a high-temperature furnace at 1 600 ℃ for 5 h. The glass melt was poured into a pre-heated copper mold at 460 ℃, allowing for rapid cooling and solidification to form transparent glass. To eliminate thermal stress, the glass was placed in a muffle furnace at 500 ℃ for 5 h and allowed to cool naturally to room temperature. The glass preparation process is shown in Fig. 1.

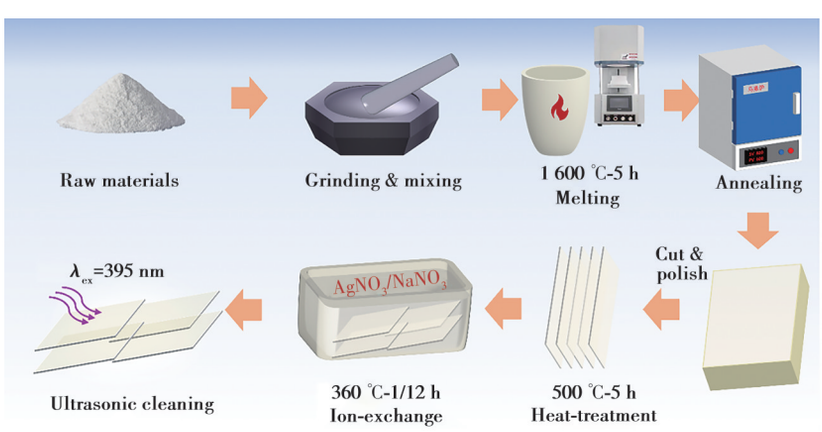

Fig. 1　Preparation and ion exchange flowchart of Sm^{3+}-doped LAS glass

The bulk glass was cut into slides with size of 10 mm×20 mm×1 mm and polished to optical quality. After polishing, the glass samples were immersed in a molten salt bath composed of $AgNO_3$ and $NaNO_3$ at a soaking temperature of 360 ℃ for durations of 1 h and 12 h, with the ratio of $c(AgNO_3)$: $c(NaNO_3)$ being 1:100, 3:100, 5:100, 7:100, and 9:100. The corresponding samples were denoted as S0Ax-1 h, S0Ax-12 h, S4Ax-1 h and S4Ax-12 h (x takes values of 1, 3, 5, 7, and 9 based on $c(AgNO_3)$). The samples were removed from the molten salt and washed with alcohol under ultrasonic conditions for 2 h to eliminate any residual nitrates on the surface.

2.2 Characterization

The absorption spectrum of the glass samples was recorded using a Lambda 750S UV-Vis spectrophotometer with a spectral resolution of 2 nm over a wavelength range of 200−800 nm. The PL spectrum of the glass was measured on a fluorescence spectrophotometer (QM/TM/NIR, PTI, USA). The transmission electron microscope (TEM, JEM-F200, JEOL, Japan) was utilized to observe the microstructure images of the samples at an accelerated voltage of 200 kV, elemental type and content analysis of the samples was conducted using an energy dispersive spectrometer (EDS, X-Max N80, Oxford Instruments, UK) attached to a transmission electron microscope. The Ag content in the glass was measured using an atomic absorption spectrometer (CONTRAA-700, AJ, Germany) under an Ar gas pressure of 0.3 MPa, and the depth of Ag ion-exchange was assessed using an electron probe microanalyzer (EPMA, JXA-8230, JEOL, Japan). The thermal stability of the sample was studied using a differential scanning calorimeter (DSC, STA 449 F3, Shimadzu, Japan), with a heating rate of 10 K/min and a temperature range from room ftemperature to 1 000 ℃ in an atmosphere of N_2. The structure of the sample was investigated using a Raman spectrometer (LABHRev-UV, HORIBA Jobin, France). A surface polished sample was used to conduct the the test with a 532 nm laser, over a range of 300−1 500 cm^{-1}.

3 Results and Discussion

To design the ion-exchange and heat-treatment temperature, the thermal properties were analysed by differential scanning calorimetry (DSC). As shown in Fig. S1(a), the glass transition temperature (T_g) of S0 sample is 524 ℃. After doping with 0.4% Sm, the T_g decreased slightly to 519 ℃. It can be seen that the incorporation of Sm^{3+} ions does not significantly affect the thermal stability of LAS glass, which can be well used in a series of performance enhancement schemes such as ion exchange.

To investigate the impact of Ag^+ ions entering the glass matrix on the microscopic structure of the glass, Raman spectroscopy was conducted on the S4A*x*-12 h sample, as shown in Fig. S1(b). Peak fitting analysis was performed on the vibration bands at 1 056 cm^{-1} and 1 270 cm^{-1}, with the corresponding results presented in Fig. S1(c). The band centered at 1 056 cm^{-1} is assigned to the symmetric stretching vibration of O-Si-O in Q4 silicate tetrahedra. The band centered at 1 154 cm^{-1} is assigned to the symmetric stretching vibration of O-Si-O in Q3 tetrahedra. Additionally, the band at 1 265 cm^{-1} is assigned to other inorganic structures in the material. Obviously, the glass structure did not change significantly, indicating that the LAS glass is stable and suitable for ion exchange.

0.4% Sm_2O_3 (S4) doped glass samples were immersed in molten salts with different concentrations of $AgNO_3$ for 1 h and 12 h and then taken out from the salts. The ion-exchanged glasses S4A5-1 h and S4A5-12 h were selected for analysis. As illustrated in Fig. 2(a), Ag^+ ions in the molten salt gradually replace Na^+ and Li^+ ions in the glass matrix, followed by reduction and aggregation to form Ag aggregates at an exchange temperature of 360 ℃. To investigate the extent of ion exchange, we measured the depth of Ag in the glass surface layer after ion exchange. As shown in Fig. 2(b), the presence of Ag can be clearly detected in the surface layer of the glass after 1 h of ion-exchange. As the proportion of $AgNO_3$ in the molten salt increases, the ion-exchange depth at the glass surface remains around 50 nm, with no significant differences observed. In fact, distinct peaks in the Ag concentration distribution can be observed in the early stages of ion-exchange, which are related to the differences in diffusion coefficients of Ag ions and sodium ions in the glass. After 1 h of ion-exchange, these distinct peaks become blurred[28]. Fig. 2(c) shows that after 12 h of ion-exchange, Ag has diffused throughout the entire glass sample, resulting in a more uniform distribution of Ag. In addition to the distribution depth of Ag in the glass after ion exchange, the oxidation state of Ag in the glass is also a matter of concern. Therefore, we tested the X-ray photoelectron spectroscopy (XPS) spectrum of S4A*x*-12 h, and the results are shown in Fig. 2(d). The binding energies of $Ag3d_{3/2}$ and $Ag3d_{5/2}$ are 374.3 eV and 368.3 eV, respectively.

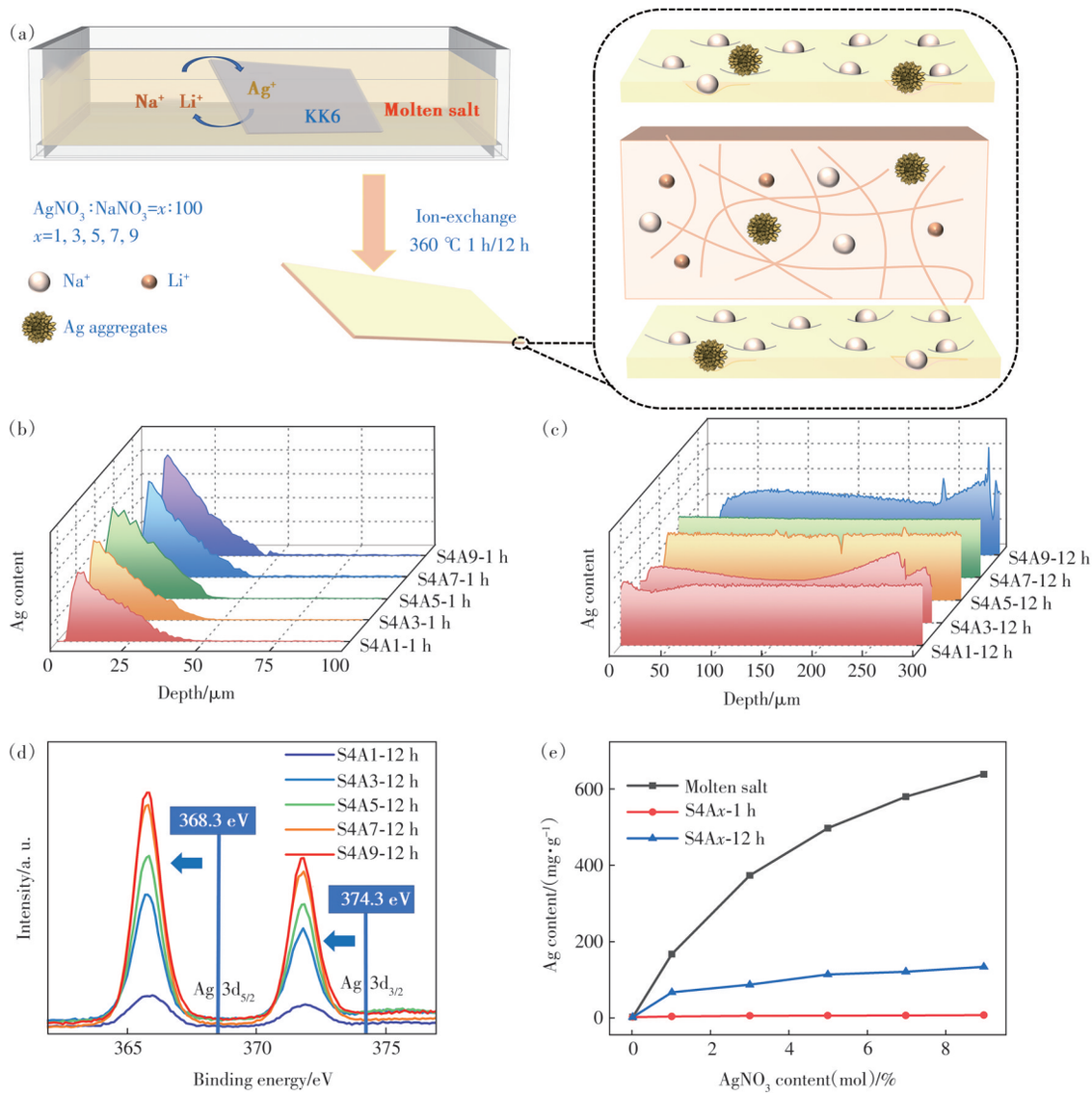

Fig. 2　(a) Schematic of ion-exchange process. Ion-exchange depth of Ag in the surface layer of S4A*x*-1 h (b) and S4A*x*-12 h (c), respectively. (d) XPS spectra of S4A*x*-12 h. (e) Ag content in molten salt and samples

The noticeable shift in the peak positions in the figure indicates that Ag exists in an oxidized state within the LAS glass. The orbital binding energy of elemental Ag decreases with increasing ionic valence, with 367.9 eV for the $3d_{5/2}$ orbital of Ag_2O and 366.5 eV for the $3d_{5/2}$ orbital of AgO, which shows that the oxidized Ag in the sample exists in the form of AgO. Fig. 2(e) shows the variation of Ag content in the samples and molten salt, with the original data presented in Tab. S1. As the $AgNO_3$ content in the molten salt increases, the diffusion rate of Ag simultaneously accelerates, resulting in more Ag^+ ions entering the glass within the same duration. Throughout the ion-exchange process, Ag^+ gradually replaces Na^+ and K^+ within the glass matrix. After 12 h, the Ag content reaches saturation, and further extension in time do not increase the Ag content in the S4A*x* samples, therefore, the duration of the ion exchange is set to 12 h.

The glass sample S4A5-1 h was measured using a TEM to observe the morphology of Ag species within the glass matrix. Fig. 3(c) and 3(g) present the TEM images of the S4A5-1 h and S4A5-1 h HT, where S4A5-1 h HT refers to the S4A5-1 h that underwent heat-treatment at 420 ℃ for 2 h. The interplanar spacing of the lattice fringes corresponding to the dark spots in the images was calculated using Fourier transform and inverse Fourier transform

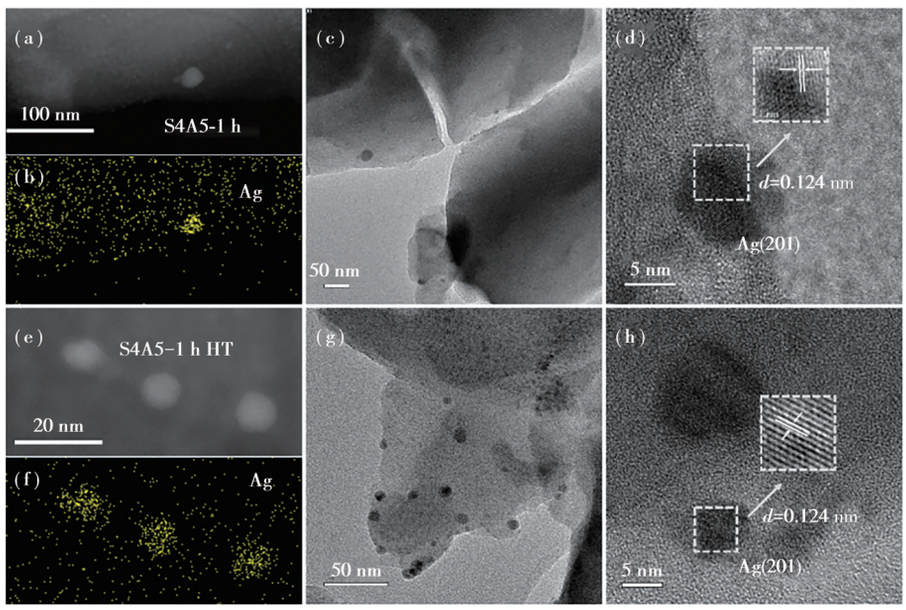

Fig. 3 Enlarged TEM image(a) and corresponding elemental mapping(b) of Ag. TEM image(c) and high-resolution TEM image (d) of S4A5-1 h. Enlarged TEM(e) and corresponding elemental mapping(f) of Ag. TEM image(g) and high-resolution TEM image(h) of S4A5-1 h HT (heat-treated)

techniques, and the results matched those of Ag, indicating that the dark spots represent Ag NPs. Fig. 3(d) and 3(h) show the (201) crystal planes of Ag, corresponding to a lattice spacing of 0.124 nm. It is generally believed that the aggregation of Ag NCs into Ag NPs occurs at temperatures above 400 ℃[29]. In samples that were not subjected to annealing heat treatment, Ag primarily exists in the form of Ag NCs or Ag^+. However, a small amount of Ag NPs was still observed in Fig. 3(c), indicating that even sample subjected to ion-exchange for as short as 1 h still contains Ag NPs. The number of Ag NPs increases and their average size grows in the heat-treated samples, suggesting that Ag^+ is reduced during the annealing process, leading to further aggregation and growth of Ag. The sizes of Ag NPs in the S4A5-1 h sample between 2 nm and 10 nm, with an average size of approximately 6 nm. In the heat-treated S4A5-1 h sample, a greater number of Ag NPs appear, with a size distribution ranging from 4 nm to 12 nm and an average size of about 7 nm.

Ag clusters cannot be directly observed using techniques such as TEM. Therefore, this study investigated the UV absorption spectrum of the samples to observe the Ag species within the samples through the absorption at different wavelengths. As shown in Fig. S4(a), absorption spectra of the 12 h ion-exchange samples (S0A0-12 h) exhibit strong absorption primarily in the 250–300 nm region, which is attributed to the intrinsic absorption of the glass matrix. The SPR absorption peak generated by the plasmonic resonance of Ag NPs at 410 nm is absent, indicating that Ag did not aggregate into nanoparticles during the ion exchange process but mainly exists in the form of Ag^+ or Ag NCs. By subtracting the absorption spectrum of S0A0 from the ion-exchange samples, the normalized absorption spectra of the ion-exchanged glasses (Fig. 4(a)) can be obtained, which effectively removes the influence of the glass matrix on the absorption and allows for a direct observation of Ag's absorption. The absorption peak of the ion-exchange glass is located around 320 nm, which is believed to be attributed to Ag NCs[30]. Qiao *et al.* suggested that the absorption band between 300 nm and 380 nm can be attributed to Ag NCs, peaking around 330 nm, which is consistent with the experimental results[31]. The absorption peaks of the glass show a trend of initially red shifting and then blue shifting with increasing Ag content, which is related to the changes in the size of the Ag aggregates during the ion-exchange process. During the ion-exchange process, Ag^+ ions enter the

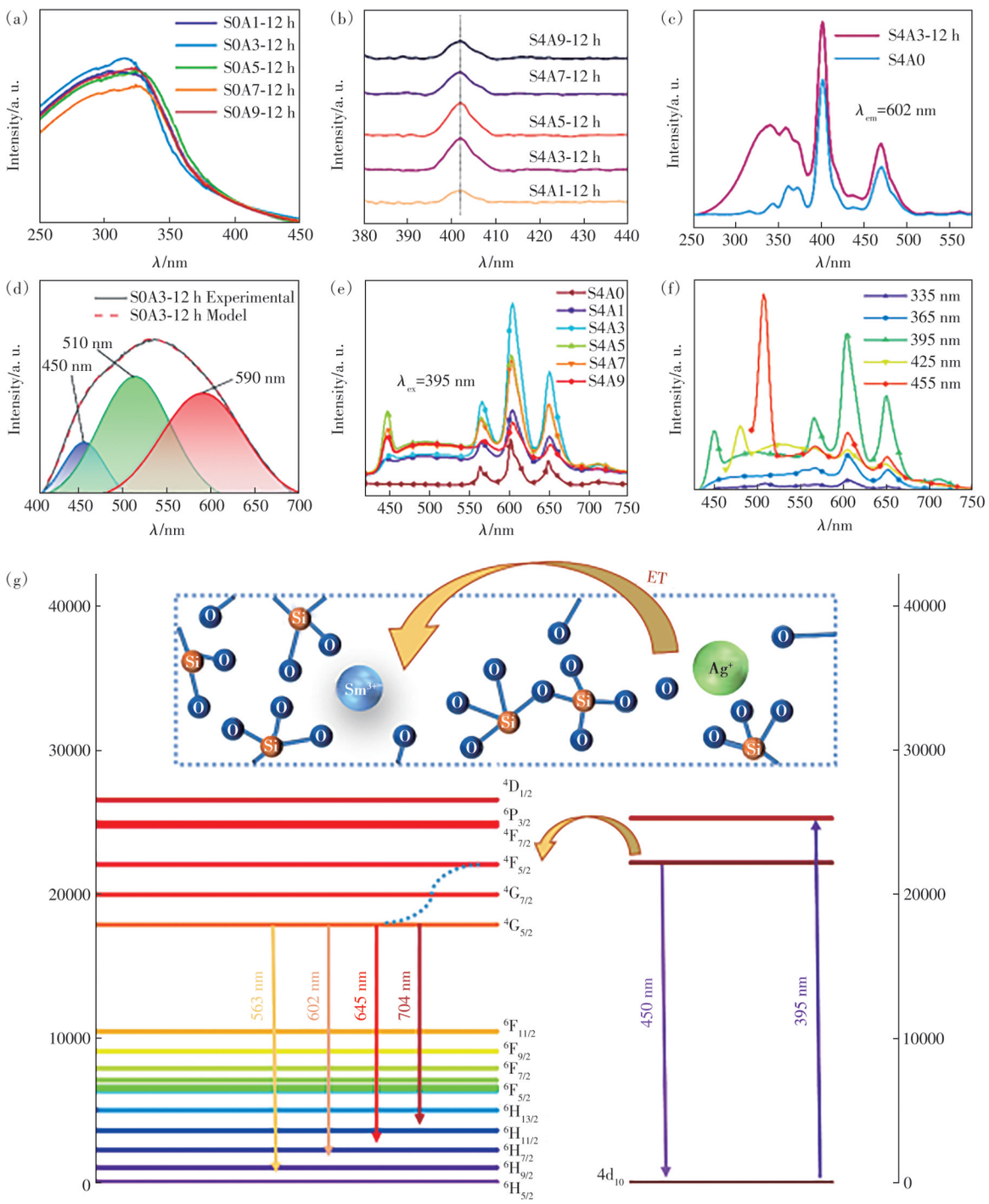

Fig. 4　(a) Absorption spectra of S0A*x*-12 h. (b) Absorption spectra of S4A*x*-12 h. (c) Excitation spectra of S4A3-12 h and S4A0 monitored at 602 nm. (d) Photoluminescence spectra of S0A3-12 h, with the red dashed line representing the deconvolution results for S0A3-12 h. (e) Photoluminescence spectra of S4A*x*-12 h under 395 nm. (f) Photoluminescence spectra of S4A5-12 h under different excitation wavelengths. (g) Energy level diagram of Ag^+ to Sm^{3+}

glass, with some coordinating with $[ZnO_4]^{2-}$ or $[AlO_4]^-$ for charge compensation. When two Ag^+ ions are situated between two $[AlO_4]^-$ or near the $[ZnO_4]^{2-}$, an (Ag^+-Ag^+) interaction can occur. Meanwhile, some Ag^+ ions find it difficult to continue dissolving within the glass network structure, resulting in aggregation outside the network. These isolated Ag^+ combine with reduced Ag^0 to form Ag dimers $(Ag_2)^+$, which progressively evolve into clusters with different structures, including $(Ag_3)^+$, $(Ag_4)^+$, and $(Ag_5)^+$. Fig. 4(b) shows the absorption spectra of S4A*x*-12h, where the absorption band centered at 401 nm is attributed to

the $^6P_{3/2}$ energy level of Sm^{3+}. Additionally, Sm^{3+} ions doped LAS glass exhibits weak absorption peaks at 360, 375, 470 nm, corresponding to the ground state $^6H_{5/2}$ to the $^4D_{3/2}$, $^6P_{7/2}$, and $^4M_{15/2}$ energy levels.

Introducing Ag into rare earth doped glass can significantly enhance the luminescent properties of rare earth ions. The excitation spectrum and luminescent spectrum can efficiently and precisely evaluate the luminescent quality of the samples. The excitation spectra of S4A0 and S4A3-12 h recorded between 250 nm and 600 nm are shown in Fig. 4(c). The excitation bands of S4A0 at 345, 363, 375, 403, 417, 438, 474, 528 nm are attributed to the electronic transitions of Sm^{3+} from $^6H_{5/2}$ to $^4H_{9/2}$, $^4D_{3/2}$, $^6P_{7/2}$, $^4F_{7/2}$, $^6P_{5/2}$, $^4G_{9/2}$, $^4I_{11/2}$, and $^4F_{3/2}$. Among these, the transition at 402 nm from $^6H_{5/2}$ to $^4F_{7/2}$ is more likely to occur and exhibits the strongest excitation intensity. Compared to S4A0, the excitation band of S4A3-12 h is significantly enhanced in the range of 250−380 nm, which can be attributed to the Ag aggregates. At this point, the luminescence of the sample primarily comes from the Ag aggregates. However, as the excitation wavelength increases, the luminescence of Sm^{3+} begins to dominate.

To investigate the luminescence of Ag, the luminescence spectrum of S0A3-12 h was collected and shown in Fig. 4(d). Under excitation at 395 nm, the S0A3-12 h sample exhibits broad band emission, which can be fitted by three peaks using Gaussian model, the peak positions are located at 450, 510, 590 nm. The emission at 450 nm primarily originates from $(Ag_2)^+$, while the emission at 510 nm is mainly associated with Ag ion pairs (Ag^+-Ag^+). The 590 nm emission corresponds to a mixture of Ag and Ag^+, predominantly appearing as $(Ag_2)^+$, $(Ag_3)^+$, or $(Ag_3)^{2+}$, atoms, or clusters.

The emission properties of ion-exchanged glass are related to the concentration, valence state, and aggregation state of Ag in the glass[32]. The presence state of Ag in the glass, in turn, is influenced by several factors, including the ion exchange temperature, duration, molten salt concentration, and the composition of the glass matrix. Therefore, by adjusting the concentration of the molten salt, samples with different emission properties can be obtained. Under 395 nm excitation, the S4A0 sample, which underwent no ion-exchange, displays multiple emission bands related to Sm^{3+}, as shown in Fig. 4(e). The emission at 565 nm corresponds to the electronic transition from $^4G_{5/2}$ to $^6H_{5/2}$, emitting yellow light, while the emission band at 602 nm is attributed to the electronic transition from $^4G_{5/2}$ to $^6H_{7/2}$, emitting orange light. Additionally, the emission band at 647 nm corresponds to the electronic transition from $^4G_{5/2}$ to $^6H_{9/2}$, emitting orange-red light. In fact, there is an emission from Sm^{3+} at 709 nm corresponding to electronic the transition from $^4G_{5/2}$ to $^6H_{11/2}$, emitting red light. Among all the emission bands, the 602 nm electronic transition from $^4G_{5/2}$ to $^6H_{7/2}$ is the predominant one, resulting in a strong orange emission in the S4A0 sample. The emission of the ion-exchanged samples at 450 nm and the broad emission in the range of 470−550 nm is attributed to a mixture of Ag^+. The PL intensity tends to increase with the increase of $AgNO_3$ ratio in the molten salt, and the intensity of the Sm^{3+} emission band reaches a maximum at 3% of $AgNO_3$ ratio, which is enhanced by a factor of 3 compared with the S4A0 sample. When the proportion of $AgNO_3$ is 5%(mole fraction), the intensity of the Ag emission band reaches its peak at 250−380 nm. The enhancement of the Sm^{3+} emission band under UV excitation is attributed to the energy transfer from Ag^+ to Sm^{3+}. Ag^+ absorbs energy from UV light, causing the outermost electrons to transition from the ground state to an excited state. Subsequently, the excited electrons relax back to the ground state, converting the relaxation energy into broad band UV emission. A portion of this energy is transferred to adjacent Sm^{3+} ions, enhancing the electronic transitions at the Sm^{3+} energy levels and thereby boosting the visible light emission[33].

To investigate the effect of excitation wavelength on the luminescent properties of the samples, the photoluminescence spectrum of S4A5-12 h was tested at excitation wavelengths of 335, 365, 395, 425, 455 nm, as shown in Fig. 4(f). It is observable that as the excitation wavelength increases, the emission band of Ag NCs at 450 nm shows a noticeable red shift, which is attributed to the fact that the excitation wavelength of 455 nm favors the luminescence

of large-sized Ag NCs such as $(Ag_5)^+$, while the excitation wavelengths of 395 nm and 425 nm favor the luminescence of $(Ag_2)^+$, Ag^+-Ag^+.

A schematic of the energy transfer process from Ag NCs to Sm^{3+} is shown in Fig. 4(g). In this process, the emission intensity of Sm^{3+} depends on the energy transfer efficiency. The short distance between Ag^+ and Sm^{3+} promotes effective energy transfer efficiency, leading to a significant enhancement of Sm^{3+} emission intensity with increasing Ag^+ concentration. However, when the Ag^+ concentration is further increased, the emission intensity begins to decrease, as the relative concentration of Sm^{3+} slightly declines alongside the increase in Ag^+. Thus, the Sm^{3+} emission intensity is ultimately influenced by both energy transfer efficiency and Sm^{3+} concentration, exhibiting a trend of initial enhancement followed by a decrease with increasing Ag^+ concentration.

The absorption spectra of S4A*x*-12 h after heat treatment at 420 ℃ for 2 h are shown in Fig. 5(a).

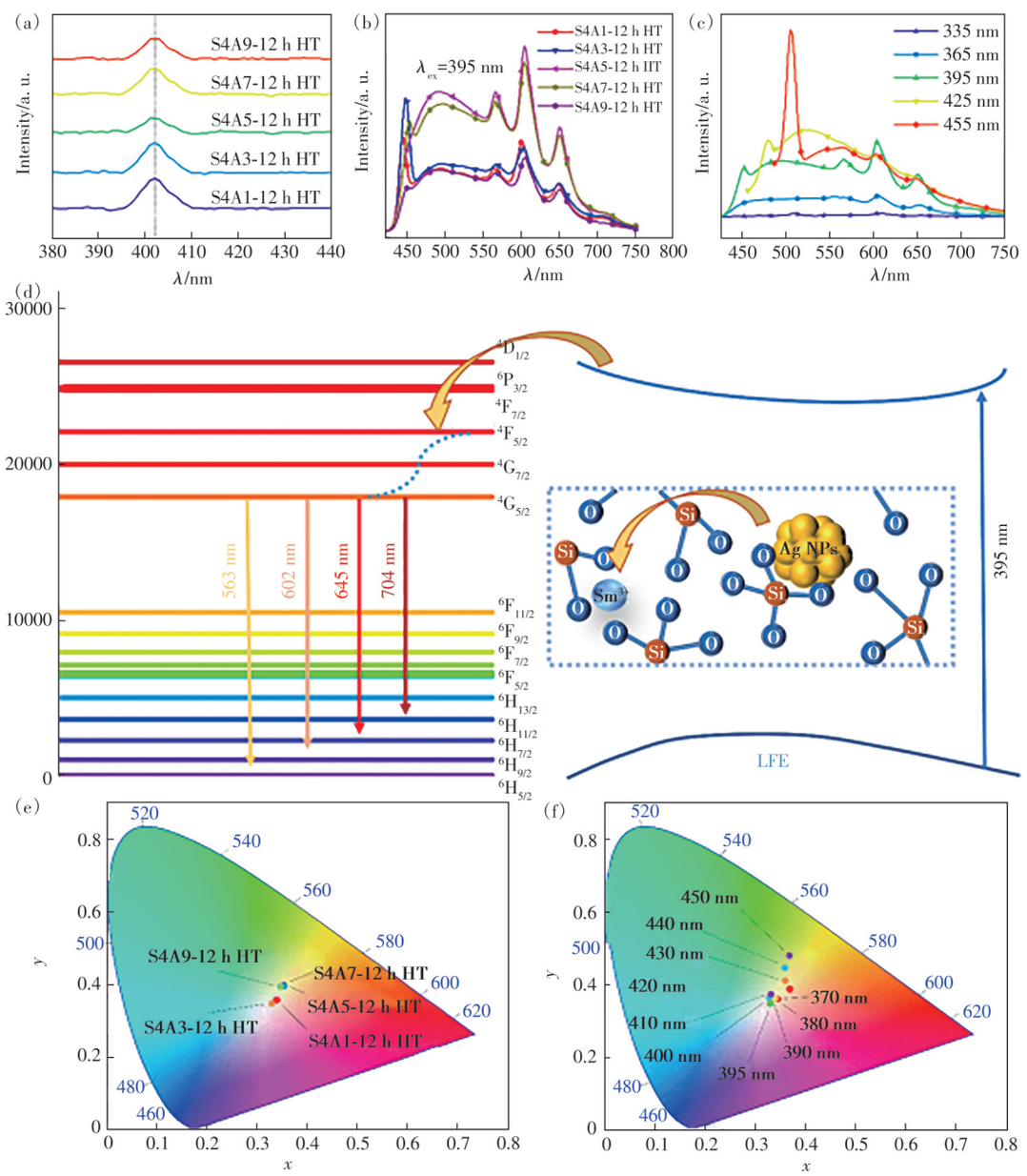

Fig. 5　(a) Absorption spectra of S4A*x*-12 h HT. (b) Luminescence spectra of S4A*x*-12 h HT under 395 nm. (c) Luminescence spectra of S4A5-12 h HT under different excitation wavelengths. (d) Illustration of energy transfer from Ag NPs to Sm^{3+}. (e) Color coordinates of the S4A*x*-12 h HT under 395 nm. (f) Color coordinates of the S4A3-12 h HT under different excitation wavelengths

Compared to that before heat treatment, the peak at 401 nm can be attributed to the SPR of Ag NPs, indicating the Ag clusters within the glass aggregated and grew into Ag NPs during the heat treatment process. This process is beneficial for enhancing the fluorescent emission of Sm^{3+}.

Different ions correspond to different peak values in the luminescence spectrum. To investigate the interaction between Sm^{3+} and Ag NPs, this study monitored the luminescence spectrum of S4A*x*-12 h HT under 395 nm excitation, as shown in Fig. 5(b). Compared to the samples that before heat treatment, S4A*x*-12 h HT exhibits a significant enhancement in the broad emission band in the range of 470–550 nm. The emission intensities corresponding to the Sm^{3+} emission bands at 565, 602, 647, 709 nm also increased. The Sm^{3+} emission band of the S4A5-12 h HT sample was enhanced by a factor of 5 compared to S4A0. However, further increasing Ag concentration led to quenching of the emission intensity. During the heat treatment process, a considerable portion of the Ag NCs grew into Ag NPs. It is well known that the oscillation of electrons gives rise to surface plasmon polaritons, which travel along the surface of the metallic particles, a phenomenon known as SPR. This generates a LFE that amplifies the electromagnetic field around Sm^{3+}, leading to enhanced fluorescence. On the other hand, the Ag NPs may weaken the enhancement of the electromagnetic field around Sm^{3+}. In other words, the excited electrons transfer energy from Sm^{3+} to Ag NPs, leading to fluorescence quenching. The close proximity of Ag NPs enhances the efficiency of energy transfer and increases multipole interactions, resulting in a continuous decrease in luminescence intensity for samples with higher Ag content. A similar observation was made after Ag^{+}-Na^{+} exchange in Tb^{3+} doped sodium-aluminosilicate glass, where Ag NPs were thought to provide a non-radiative pathway for energy loss caused by the electronic excitation of Tb^{3+} ions[34].

The extended heat treatment process promotes the growth of Ag NCs into larger Ag NPs. Smaller Ag NCs are continuously consumed, but the formation of new smaller Ag NCs within the glass matrix is quite limited. As a result, the number of Ag NCs decreases during the ongoing process of consumption and generation, leading to a reduction in the emission intensity corresponding to Ag in the 425–550 nm range. As previously reported, the PL intensity of Ag slightly decreases under 340–380 nm excitation when the Sm^{3+} concentration reaches 0.8%, as most of the Ag NCs grow into non-luminescent Ag NPs[35].

Fig. 5(c) displays the emission spectra of the S4A5-12h HT sample under excitation wavelengths of 335, 365, 395, 425, 455 nm. The results indicate a noticeable red shift in the emission bands of Ag NCs, accompanied by a significant increase in emission. The redshift of the emission band is attributed to the change in excitation wavelength, while the enhancement of the emission band is mainly due to the SPR effect of Ag NPs. As illustrated in the energy level diagram in Fig. 5(d), electrons in the ground state of Sm^{3+} were excited to the $^4F_{7/2}$ state through ground state absorption (GSA) under 407 nm excitation, followed by a relaxation process to populate the excited state $^4G_{5/2}$ through multiphonon non-radiative decay. Simultaneously, the 407 nm excitation light resonates due to the LFE produced by the Ag NPs, generating a strong and highly localized electric field around the Ag NPs through SPR. This LEF enhances the radiative transition probability of Sm^{3+} ions near the Ag NPs, thereby intensifying the emission band. Conversely, luminescence quenching is ascribed to energy transfer from Sm^{3+} ions to Ag NPs and optical reabsorption by non-plasmonic species. Although a large number of Ag NCs in the heat-treated samples grew to Ag NPs, a portion of Ag still existed in the form of ions and clusters, so the phenomenon of enhanced luminescence of Sm^{3+} due to energy transfer from Ag^{+} to Sm^{3+} within the heat-treated samples still existed.

The above results demonstrate that the emission band of the ion-exchange samples can be tailored through adjustments the excitation wavelength and Ag concentration. Consequently, these manipulations enable modulation of the corresponding color coordinates of the samples. The color coordinates of

S4A*x*-12 h HT is plotted on the CIE 1931 chromaticity diagram, as shown in Fig. 5(e). Under excitation at 395 nm, the color coordinate of S4A3-12 h HT is recorded as (0.33, 0.34), which is very close to the equal energy white point E (0.33, 0.33), and the CRI reaches a value of 81.8. Additionally, the color coordinates of S4A1-12h HT are found to be (0.33, 0.36), demonstrating excellent white light emission performance. As the Ag concentration increases, the color coordinates shift towards the warm yellow light, which is related to the growth of Ag clusters in the samples. Fig. 5(f) displays the variation of the color coordinates of the S4A3-12 h HT sample under different excitation wavelengths. It can be observed that as the excitation wavelength increases from 370 nm to 450 nm, the emission color shifts from the warm white to the cool white, and then returns to the warm white. This indicates that the luminescent color of the Ag aggregates/Sm^{3+} can be effectively tuned to achieve white light emission by altering the excitation wavelength.

4 Conclusion

In summary, a series of Ag^{+}/Sm^{3+} co-doped LAS glasses were prepared using the melting quenching method. TEM and EDS revealed the presence of Ag in a morphological way within the glass matrix, while the absorption spectra further confirmed that Ag primarily exists in ionic form in the ion-exchanged samples. It was observed that the glass containing Ag aggregates exhibited strong broadband emission along with red emission from Sm^{3+}. By adjusting the ratio of Ag to Sm^{3+} in the glass matrix, a series of tunable white fluorescence emissions can be achieved. Under 395 nm excitation, the color coordinates of the S4A3-12 h HT are located at (0.33, 0.34), and the CRI reached a value of 81.8. As the excitation wavelength increased from 370 nm to 450 nm, the color coordinates of the glass fluorescence shifted from (0.34, 0.36) to (0.33, 0.34), and then towards (0.36, 0.38), indicating that altering the excitation wavelength can effectively tune the luminescent color of the Ag aggregates/Sm^{3+} and thereby achieve white light emission.

Supplementary Information and Response Letter are available for this paper at: http://cjl.lightpublishing.cn/thesisDetails#10.37188/CJL.20250047

References:

[1] ZHOU B, TAO L L, CHAI Y, *et al.* Constructing interfacial energy transfer for photon up-and down-conversion from lanthanides in a core-shell nanostructure [J]. *Angew. Chem., Int. Ed.*, 2016, 55(60): 12356-12360.

[2] DONG H, SUN L D, YAN C H. Energy transfer in lanthanide upconversion studies for extended optical applications [J]. *Chem. Soc. Rev.*, 2015, 44: 1608-1634.

[3] LIANG L L, FENG Z W, ZHANG Q M, *et al.* Continuous-wave near-infrared stimulated-emission depletion microscopy using downshifting lanthanide nanoparticles [J]. *Nat. Nanotechnol.*, 2021, 16(9): 975-980.

[4] JIANG Z, HE L R, YANG Z W, *et al.* Ultra-wideband-responsive photon conversion through co-sensitization in lanthanide nanocrystals [J]. *Nat. Commun.*, 2023, 14(1): 827.

[5] WU S L, XIA H B, XU J H, *et al.* Manipulating luminescence of light emitters by photonic crystals [J]. *Adv. Mater.*, 2018, 30(47): 1803362.

[6] STEUDEL F, LOOS S, AHRENS B, *et al.* Luminescent borate glass for efficiency enhancement of CdTe solar cells [J]. *J. Lumin.*, 2015, 164: 76-80.

[7] BOUCCARA S, SITBON G, FRAGOLA A, *et al.* Enhancing fluorescence *in vivo* imaging using inorganic nanoprobes [J]. *Curr. Opin. Biotechnol.*, 2015, 34: 65-72.

[8] DEOPA N, RAO A S. Spectroscopic studies of Sm^{3+} ions activated lithium lead alumino borate glasses for visible luminescent device applications [J]. *Opt. Mater.*, 2017, 72: 31-39.

[9] CHEN B J, SHEN L F, PUN E Y B, *et al.* Sm^{3+}-doped germanate glass channel waveguide as light source for minimally invasive photodynamic therapy surgery [J]. *Opt. Express*, 2012, 20(2): 879-889.

[10] ELISA M, SAVA B A, VASILIU I C, *et al.* Optical and structural characterization of samarium and europium-doped

phosphate glasses [J]. J. *Non-Cryst. Solids*, 2013, 369: 55-60.

[11] SHANMUGA SUNDARI S, MARIMUTHU K, SIVRAMAN M, *et al*. Composition dependent structural and optical properties of Sm^{3+}-doped sodium borate and sodium fluoroborate glasses [J]. *J. Lumin.*, 2010, 130(7): 1313-1319.

[12] SELVAN S T, HAYAKAWA T, NOGAMI M. Remarkable influence of silver islands on the enhancement of fluorescence from Eu^{3+} ion-doped silica gels [J]. *J. Phys. Chem.* B, 1999, 103(34): 7064-7067.

[13] KASSAB L R P, BOMFIM F A, MARTINELLI J R, *et al*. Energy transfer and frequency upconversion in Yb^{3+}-Er^{3+}-doped PbO-GeO_2 glass containing silver nanoparticles [J]. *Appl. Phys.* B, 2009, 94(2): 239-242.

[14] KINDRAT I I, PADLYAK B V, KUKLIŃSKI B, *et al*. Enhancement of the Eu^{3+} luminescence in $Li_2B_4O_7$ glasses co-doped with Eu and Ag [J]. *J. Lumin.*, 2018, 204: 122-129.

[15] EICHELBAUM M, RADEMANN K. Plasmonic enhancement or energy transfer? On the luminescence of gold-, silver-, and lanthanide-doped silicate glasses and its potential for light-emitting devices [J]. *Adv. Funct. Mater.*, 2009, 19(13): 2045-2052.

[16] JIMÉNEZ J A. Temperature dependence of Cu^{+} luminescence in barium-phosphate glasses: Effect of rare-earth ions (Sm^{3+}, Nd^{3+}) and correlation with glass structure [J]. *J. Non-Cryst. Solids*, 2016, 432: 227-231.

[17] LI J J, WEI R F, LIU X Y, *et al*. Enhanced luminescence via energy transfer from Ag^{+} to RE ions (Dy^{3+}, Sm^{3+}, Tb^{3+}) in glasses [J]. *Opt. Express*, 2012, 20(9): 10122-10127.

[18] SANDRINI M, MUNIZ R F, ZANUTO V S, *et al*. Enhanced and tunable white light emission from Ag nanoclusters and Eu^{3+}-co-doped CaBAl glasses [J]. *RSC Adv.*, 2018, 8(61): 35263-35270.

[19] WANG H Q, BATENTSCHUK M, OSVET A, *et al*. Rare-earth ion doped up-conversion materials for photovoltaic applications [J]. *Adv. Mater.*, 2011, 23(22-23): 2675-2680.

[20] GOUVEIA-NETO A S, RIOS N P S M, BUENO L A. Spectroscopic study and white-light simulation using praseodymium-doped fluorogermanate glass as single phosphor for white LEDs [J]. *Opt. Mater.*, 2012, 35(2): 126-129.

[21] REN L J, LEI X H, DU X Q, *et al*. Effect of Eu_2O_3 concentration on luminescent properties of Ce/Tb/Eu co-doped calcium borosilicate glass for white LED [J]. *J. Lumin.*, 2013, 142: 150-154.

[22] ATUCHIN V V, YELISSEYEV A P, GALASHOV E N, *et al*. Synthesis and luminescence properties of Li_2O-Y_2O_3-TeO_2: Eu^{3+} tellurite glass [J]. *Mater. Chem. Phys.*, 2014, 147(3): 1191-1194.

[23] LIU Y F, HOU X Y, SONG Y L, *et al*. Bioinspired reflective display based on photonic crystals [J]. *Interdiscip. Mater.*, 2024, 3(1): 54-73.

[24] ZHAO J Y, ZHU J L, YANG Z W, *et al*. Selective preparation of Ag species on photoluminescence of Sm^{3+} in borosilicate glass *via* Ag^{+}-Na^{+} ion exchange [J]. *J. Am. Ceram. Soc.*, 2020, 103(2): 955-964.

[25] SORIANO-ROMERO O, JUÁREZ-RAYÓN I, CARMONA-TÉLLEZ S, *et al*. Multicolor emission in Ag_m^{n+} clusters and Eu^{3+} activated ZnO-P_2O_5 glasses achieved under near ultraviolet light excitation [J]. *Opt. Mater.*, 2022, 123: 111833.

[26] 魏东, 苏文霞. 白光LEDs用掺杂Eu^{2+}和Mn^{2+}的$CaAlSiN_3$荧光粉合成及发光性能改进 [J]. 发光学报, 2024, 45(10): 1656-1666.
WEI D, SU W X. Synthesis and luminescence improvement of $CaAlSiN_3$ phosphors doped with Eu^{2+} and Mn^{2+} for white LEDs [J]. *Chin. J. Lumin.*, 2024, 45(10): 1656-1666. (in Chinese)

[27] 陈蕾, 杨星宇, 张瀚月, 等. $NaYSiO_4$:Ce^{3+}蓝色荧光粉的发光性质及其在白光发光二极管上的应用 [J]. 发光学报, 2024, 45(5): 745-752.
CHEN L, YANG X Y, ZHANG H Y, *et al*. Photoluminescence properties and white light emitting diodes applications of $NaYSiO_4$:Ce^{3+} blue phosphor [J]. *Chin. J. Lumin.*, 2024, 45(5): 745-752. (in Chinese)

[28] LIHACHEV A I, NASHCHEKIN A V, SOKOLOV R V, *et al*. Determination of the thicknesses and visualization of ion-exchange waveguides in glasses by scanning electron microscopy [J]. *Tech. Phys.*, 2019, 64(3): 418-421.

[29] NIKONOROV N V, IVANOV S A, MUSIKHINA E S. Photo-thermo-refractive glass: a promising photonics material [Review] [J]. *J. Opt. Technol.*, 2023, 90(3): 142-160.

[30] LOGINOV E, GOMEZ L F, CHIANG N, *et al*. Photoabsorption of Ag_N ($N \sim 6$–$6\,000$) nanoclusters formed in helium droplets: transition from compact to multicenter aggregation [J]. *Phys. Rev. Lett.*, 2011, 106(23): 233401.

[31] MA R H, ZHAO J J, CHEN X T, *et al*. Stabilization of ultra-small $[Ag_2]^{2+}$ and $[Ag_m]^{n+}$ nano-clusters through negatively charged tetrahedrons in oxyfluoride glass networks: To largely enhance the luminescence quantum yields [J]. *Phys.*

Chem. Chem. Phys., 2017, 19(34): 22638-22645.

[32] PAJE S, GARCÍA M A, LLOPIS J, *et al.* Optical spectroscopy of silver ion-exchanged As-doped glass [J]. *J. Non-Cryst. Solids*, 2003, 318(3): 239-247.

[33] ZHANG L L, XIA Y, SHEN X, *et al.* A significant enhancement emission of Sm^{3+}-Ag^{+} codoped silicate glasses under UV excitation [J]. *J. Mater. Res.*, 2018, 33(16): 2434-2439.

[34] LI L J, YANG Y, ZHOU D C, *et al.* The influence of Ag species on spectroscopic features of Tb^{3+}-activated sodium-aluminosilicate glasses *via* Ag^{+}-Na^{+} ion exchange [J]. *J. Non-Cryst. Solids*, 2014, 385: 95-99.

[35] MECHERGUI I, FARES H, MOHAMED S A, *et al.* Coupling between surface plasmon resonance and Sm^{3+} ions induced enhancement of luminescence properties in fluoro-tellurite glasses [J]. *J. Lumin.*, 2017, 190: 518-524.

常元星(2001-),女,贵州铜仁人,硕士,2025年于武汉理工大学获得硕士学位,主要从事稀土离子掺杂发光玻璃的研究。

E-mail: 307395445@qq.com

许银生(1984-),男,甘肃威武人,博士,研究员,博士生导师,2011年于华东理工大学和法国雷恩第一大学获得博士学位,主要从事红外玻璃和光纤以及发光材料与器件的研究。

E-mail: xuyinsheng@whut.edu.cn